Dating folding beyond folding, from layer-parallel shortening to fold tightening, using mesostructures: Lessons from the Apennines, Pyrenees and Rocky Mountains.

Olivier Lacombe[1], Nicolas E. Beaudoin[2], Guilhem Hoareau[2], Aurélie Labeur[2], Christophe Pecheyran[3], Jean-Paul Callot[2]

1. Sorbonne Université, CNRS, Institut des Sciences de la Terre de Paris, Paris, France

2. Universite de Pau et des Pays de l'Adour, E2S UPPA, CNRS-TOTAL, LFCR, Pau, France

3. Universite de Pau et des Pays de l'Adour, E2S UPPA, IPREM, Pau, France

Abstract

Dating syntectonic sedimentary sequences is often seen as the unique way to constrain the initiation, duration and rate of folding as well as the sequence of deformation in the shallow crust. Beyond fold growth however, deformation mesostructures accommodate the internal strain of pre-folding strata before, during and after strata tilting. Absolute dating of syn-folding mesostructures may help constrain the duration of fold growth in the absence of preserved growth strata, while dating of mesostructures related to early-folding layer-parallel shortening and late fold tightening provide a valuable access to the timing and duration of the entire folding event. We compile existing ages in the literature and provide new U-Pb ages of calcite cements from veins and faults from four folds (Apennines, Pyrenees, Rocky Mountains). Our results not only better constrain the timing of fold growth but also reveal a contraction preceding and following folding, the duration of which might be a function of the tectonic style and regional sequence of deformation. This study paves the way for a better appraisal of folding lifetime and processes and of stress evolution in folded domains.

1. Introduction

Quantifying the rates and duration of deformation processes is key to understand how the continental crust deforms. Quite a lot is known about rates and duration of ductile deformation in the lower crust, for instance that shear zones can be active for 10s or 100s My (Schneider et al., 2013; Mottram et al., 2015). However, less is known about the duration and rates of folding processes in the upper crust. Short-term folding rates are usually captured by studying deformed terraces and alluvial fan ridges associated with active folds, and the dating of the inception and lifetime of folds is based on the extrapolation of these short-term rates back in time assuming a steady deformation rate.

The other classical mean to constrain the age and rate of upper crustal folding consists in dating growth strata. In orogenic forelands, contractional deformation causes folding of the pre-deformational sedimentary sequence and when sedimentation occurs continuously during deformation, growth strata are deposited synchronously with folding. Growth strata often show a characteristic pattern, such as decreasing dips up section toward the limbs of the fold, fan-like geometry and unconformities (Riba, 1976; Fig.1). Several factors control growth strata patterns, such as kink-band migration, fold uplift, limb rotation and lengthening rates, as well as sedimentation and erosion rates (Suppe et al., 1992; Storti and Poblet, 1997). Chronostratigraphic constraints are critical for defining the duration and rate of fold growth (Butler and Lickorish, 1997). Dating the base of the growth strata defines the youngest initiation age for the fold, while post-growth strata conceal the final geometry of the fold and mark the end of folding (Fig.1).

However, preserved growth strata are not ubiquitous/are rare, and the folded multilayer typically includes only pre-growth strata. Also, the fold growth may be highly discontinuous through time, deformation being episodic at all timescales with tectonic uplift pulses of different duration and intensity interrupted by periods of variable extent in which no fold growth occurred (Masaferro et al., 2002; Carrigan et al., 2016; Anastasio et al., 2018). Where available, the study of syntectonic unconformities (Barnes, 1996) or terraces (Mueller and Suppe, 1997) otherwise suggest that the growth of some folds may be caused by earthquake-related slip on active faults, which is by essence discontinuous. These studies emphasize the difficulty to extrapolate fold growth rates back in time. The age of fold initiation

obtained by assuming steady shortening rate, deposition rate and fold growth rate is therefore at best strongly biased, at worst false, so the duration of fold growth remains poorly constrained.

Folding is also accompanied by deformation mesostructures such as faults, joints and veins, and stylolites (e.g. Tavani et al., 2015, and references therein) which accommodate the internal strain of strata during folding, but also before strata started to be tilted and after tilting when shortening can no longer be accommodated by fold growth (Fig.1). Several deformation stages can typically be identified in folded pre-compressional strata, starting with pre-shortening extension related to foreland flexure and bulging, followed by layer-parallel shortening (LPS, horizontal shortening of flat-lying strata) (Amrouch et al., 2010a; Callot et al., 2010; Lacombe et al., 2011; Tavani et al., 2006, 2008, 2011, 2012; Rocher et al., 2000; Beaudoin et al., 2012, 2016; Branellec et al., 2015). Continuing horizontal stress loading and shortening usually leads to folding, associated with strata tilting and curvature and accommodated by flexural slip in the fold limbs and tangential longitudinal strain (outer arc extension and inner arc compression) in the fold hinge. The fold 'locks' when limb rotation and/or kink-band migration cannot accommodate shortening anymore. At that stage, strata tilting is over but continuous horizontal shortening leads to late stage fold tightening (LSFT), accommodated by late mesostructures developing irrespective of bedding dip (Fig. 1) (Amrouch et al., 2010a; Tavani et al., 2015). Yet, despite recent efforts (Wang et al., 2016; Grobe et al., 2019; Curzi et al., 2020; Cruset et al., 2020, 2021), the dating of the early-, syn- and late-folding mesostructures has received poor attention, although it is key to constrain not only the absolute timing of folding in the absence of growth strata, but also the entire duration of the fold-related contractional stages and the associated stress evolution from build-up to release.

We explore hereinafter the possibility to define the age and duration of folding by investigating how and for how long pre-folding strata have been accommodating shortening from the onset to the end of the horizontal contraction from which the fold originated, an event we define as the folding event (Fig. 1). This approach will better constrain the duration of fold growth by dating the syn-folding mesostructures, but also by bracketing fold growth age by dating mesostructures that immediately predate and postdate strata tilting. Doing so also enables to capture the duration of the LPS and LSFT,

two stages which have been overlooked since they accommodate much less shortening than folding itself, while being key periods of time for large scale fluid flow and related ore deposition in fold-thrust belts and sedimentary basins (e.g., Roure et al., 2005; Evans and Fischer, 2012; Beaudoin et al., 2014). For this purpose, we consider four natural folds for which we either compile existing data or provide new estimates of the age of LPS, fold growth and LSFT. Three of our examples are from fold-and-thrust belts (Apennines, Pyrenees), and one from the Laramide basement-cored folding province (Rocky Mountains). We show that mesostructures can be used to constrain the timing and duration of fold growth and/or of shortening preceding and following folding. Our results not only provide new estimates of the duration of folding, but also establish that the overall duration of the folding event may strongly vary as a function of the tectonic style of deformation, paving the way to a better mechanical appraisal of contractional deformation and stress evolution in folded domains.

2. Methods for dating the folding event using mesostructures

In this paper, we focus on easily recognizable mesostructures that develop in the same contractional stage and under the same regional trend of horizontal shortening than folding. We do not report hereinafter on microscale features (eg, calcite twins : Craddock et al., 1993; Lacombe et al., 2007, 2009; Rocher et al., 1996; Hnat et al., 2011; see review by Lacombe, 2010) or rock physical properties such as anisotropy of magnetic susceptibility (e.g, Aubourg et al., 2010; Amrouch et al., 2010b; Branellec et al., 2015, Weil and Yonkee, 2012) which have also been shown to be suitable recorders of the stress and strain history of folded strata (Lacombe et al., 2012) but the precise dating of which remains out of reach to date.

In the four folds that we investigated, the sequence and age of mesostructures were established by various dating approaches, of which methodologies are briefly recalled below (Fig.2). Note that strata from which mesostructures were dated are mainly pre-folding strata, and that there have been few (if any) attempts at directly dating mesostructures that developed within growth strata reported in the literature. The reason is that the often poorly indurated syn-folding formations are less prone to fracturing and calcite cementation at the time of deformation compared to pre-folding, well-indurated

formations, which is evidenced by the paucity of fracture studies in syn-tectonic strata (e.g., Shackleton et al., 2011).

2.1 Sequence of mesostructures related to the fold history

The characterization of the sequence of deformation was based on field measurements of stylolites and fractures and their grouping into sets according to their statistical orientation, deformation mode and relative chronology established from abutting and crosscutting relationships (Fig.2A). Their timing with respect to fold growth (i.e., early, syn-, and late folding mesostructures) was further established by considering their current and unfolded attitude at fold hinge and limbs (eg., Beaudoin et al, 2012, 2016; Tavani et al., 2015) (Fig.1).

Field observations (eg., Bellahsen et al., 2006; Ahmadhadi et al., 2008; Tavani et al., 2015) and numerical modelling (Guiton et al., 2003; Sassi et al., 2012) have emphasized the widespread reactivation during folding of fractures formed during pre-folding stages. The role of reactivation should not be, and has not been, overlooked in our study; however, for the sake of reliable absolute dating we focused on fractures the characteristics of which support that they newly formed at each deformation stage and show no textural or petrographic evidence of multiple opening or shearing events, neither at the macro- nor at the micro-scale.

2.2 Dating veins and faults

Calcite-bearing veins and faults (Fig.2A) can be dated by combining the absolute precipitation temperature of the fluids from which calcite cements formed as given by carbonate clumped isotope Δ_{47} thermometry with the burial-time history of strata (Fig.2B,D). Provided that (1) cementation was nearly coeval with fracturing, (2) the geotherm can be reliably estimated and (3) stable isotope geochemistry points towards fluid precipitation at thermal equilibrium with the host, clumped isotope thermometry of cements combined to strata burial history yields the absolute timing of the successive vein sets, hence the timing of the related deformation stages (Fig.2D) (Labeur et al., 2021).

Calcite cements can also be directly dated by carbonate geochronology (Fig.2B). Laser ablation–inductively coupled plasma–mass spectrometry (LA-ICP-MS) U-Pb dating of calcite consistently

reveals the age of brittle deformation events (Roberts and Walker, 2016; Nuriel et al., 2017; Hansman et al., 2018; Beaudoin et al., 2018; Roberts et al., 2020)(Fig.2B,D), provided that cementation was coeval with fracturing and that no later fluid infiltration and/or calcite recrystallization occurred (Roberts et al., 2021).

2.3 Combining sedimentary stylolite roughness inversion for paleodepth and burial history to constrain the onset of LPS

The onset of LPS corresponds to the time at which the maximum principal stress $\sigma 1$ switched from being vertical and related to compaction and/or to foreland flexure extension to being horizontal in response to tectonic contraction (Beaudoin et al., 2020a). In order to constrain the timing of this switch, our approach relies on the capability of bedding-parallel, sedimentary stylolite (Fig.2A) to fossilize the magnitude of the vertical stress $\sigma 1$ at the time dissolution stopped. Indeed, signal analysis (e.g. wavelets) of the final roughness of a sedimentary stylolite returns scale-dependent power laws, of which the transition length (crossover length Lc) scales with the magnitude of the vertical stress $\sigma 1$ (Schmittbuhl et al, 2004; Toussaint et al., 2018) (Fig.2C). By analyzing a population of sedimentary stylolites with this inversion technique which has been validated in numerous studies (Ebner et al., 2009; Rolland et al., 2014; Bertotti et al., 2017; Beaudoin et al., 2016, 2019, 2020a,b), one can estimate the maximum burial depth at which pressure solution was active, with 12% uncertainty (Rolland et al., 2014). Comparing this depth with the burial-time evolution of the strata as derived from well data and/or exposed stratigraphic successions provides access to the time at which compaction-driven pressure solution halted in the rock because of the switch of the maximum principal stress $\sigma 1$ from vertical to horizontal, thus revealing the age of the onset of LPS (Fig. 2D). The validity of such an approach has been established by the comparison of the age of the onset of LPS determined this way to the oldest U-Pb absolute age of LPS-related cemented fractures (Beaudoin et al., 2020a).

3. Dating natural folding events

3.1 Cingoli and San Vicino Anticlines (Apennines)

The San Vicino and Cingoli anticlines belong to the Umbria-Marche Apennine Ridge (UMAR, Fig. 3A). Apenninic deformation occurred by the Tortonian in the west of UMAR to the late Messinian-early Pliocene in the east, reaching the Adriatic domain in the late Pliocene-Pleistocene (Calamita et al., 1994). UMAR undergoes post-orogenic extension since ~3 Ma, being younger eastward and marked by recent or active normal faults cutting through the nappe stack (Barchi, 2010). The San Vicino and the Cingoli anticlines involve platform carbonates overlain by hemipelagic succession detached above Triassic evaporites and formed in late Messinian-early Pliocene (~6-5 Ma) as indicated by growth strata in the nearby Aliforni syncline (Fig.3B), following a period of foreland flexure-related extension marked by pre-contractional normal faults associated with turbidite deposition lasting until early Messinian (~6.5 Ma) (Calamita et al., 1994; Mazzoli et al., 2002).

Field analysis in the Cingoli and San Vicino fault-bend anticlines (Fig.3B) has revealed three main sets of mesostructures (Beaudoin et al., 2020b; Labeur et al., 2021). Set I consists of vertical veins perpendicular to both bedding and fold axis and striking NE-SW, associated with bed-perpendicular tectonic stylolites with peaks trending NE-SW and plunging parallel to bedding dip which, after unfolding, indicates NE-SW-directed LPS. Set II veins are bed-perpendicular and strike NW-SE, parallel to the fold axis; they abut or cut across set I veins and formed in response to outer-arc extension at fold hinge. Set III comprises NE-SW striking veins closely associated with tectonic stylolites with horizontal peaks trending NE-SW - both veins and tectonic stylolites being vertical regardless of the bedding dip - and with conjugate vertical strike-slip faults which formed during a post-tilting horizontal NE-SW contraction, i.e., LSFT (Fig.3C).

Labeur et al (2021) focused on the Cingoli anticline to reconstruct the burial history of the early Cretaceous Maiolica Fm. and Paleocene Scaglia Rossa Fm. These authors carried out an extensive inversion of the roughness of sedimentary stylolites from these formations to constrain the maximum depth at which compaction-related dissolution was active. The results are shown in Fig.3D, together with the timing of veins from sets I and II as deduced from Δ_{47} thermometry (Labeur et al., 2021) by

187 considering a 23°C/km geotherm (Caricchi et al. 2015) and a 10°C surface temperature. The resulting
188 timing for LPS, fold growth and LSFT is shown in Fig.3F.

189 To extend the published dataset to the San Vicino Anticline, veins from sets I, II and III were
190 sampled in the Cretaceous Maiolica Fm. to perform U-Pb analyses for absolute dating. Selected veins
191 display antitaxial, elongated-blocky or blocky textures (Bons et al., 2012) ensuring that the cements
192 precipitated during, or soon after, vein opening. Cathodoluminescence observations further support the
193 homogeneity of the cements (Fig.4) as well as the absence of any vein re-opening and calcite
194 recrystallization or fluid infiltration that might cause anomalous younger (reset) ages (Roberts et al.,
195 2021). U-Pb dating of calcite cements was conducted using LA-ICP-MS at the Institut des Sciences
196 Analytiques et de Physico-Chimie pour l'Environnement et les Matériaux (IPREM) laboratory (Pau,
197 France). Ages were determined from the total−Pb/U−Th algorithm of Vermeesch (2020), are quoted at
198 95% confidence, and include propagation of systematic uncertainties. Sample information, detailed
199 methodology and results are provided in the Supplemental Material. Three veins from the San Vicino
200 anticline yielded reliable ages: 6.1 ± 2 Ma for the set I vein, 3.5 ±1 Ma for the set II vein and 3.7 ± 0.3
201 Ma for the set III vein (Fig. 3E). The large uncertainties on the U-Pb age from the set II vein lead to
202 some overlap with the dates of set I and set III veins (Fig.3F). However, these veins have not only
203 distinctive orientations and consistent relative chronology, but they also have distinctive C and O stable
204 isotopic signatures of their cements while being sampled in the same part of the fold (Beaudoin et al.,
205 2020b), which supports that these veins were not cemented by the same fluid, hence were not cemented
206 coevally. The absolute vein ages, combined with existing time constraints (Fig.3F), indicate that LPS
207 occurred from ~6.5 to 5.5 Ma for both anticlines, followed by fold growth between ~5.5 and ~3.5 Ma,
208 with a seemingly slightly longer duration in Cingoli than in San Vicino. LSFT started ~5 Ma in the
209 Camerino syncline (Beaudoin et al., 2020b), ~4.5 Ma in San Vicino and ~3 Ma in Cingoli, and possibly
210 lasted until the onset of post-orogenic extension in eastern UMAR (~2.5-2 Ma, Fig.3F). The entire
211 folding event was thus very short, having lasted 3-4 My considering both anticlines as a whole (Fig.3F).

212 *3.2 Pico del Aguila Anticline (Pyrenees)*

213 The Pico del Aguila is a N160°E trending anticline in the southern Pyrenees (Fig. 5A), markedly
214 oblique to the south-Pyrenean thrust front. It formed in response to Pyrenean thrusting and detachment
215 folding above Triassic evaporites (Poblet and Hardy, 1995; Vidal Royo et al., 2009, Fig. 5B). Growth
216 strata (Fig.5B) indicate that the fold developed by late Lutetian-Priabonian (~ 42-35 Ma, Hogan and
217 Burbank, 1996), before it was passively tilted and transported southward over the Guarga basement
218 thrust (Jolivet et al., 2007).

219 Beaudoin et al. (2015) investigated the fracturing history of the Pico del Aguila (Fig. 5C). Three
220 sets of bed-perpendicular joints/veins, oriented N080°E, N060°E and N045°E (from the oldest to the
221 youngest as established from abutting/cross cutting relationships) formed in progressively younging
222 strata under a stable, far-field NE-SW shortening while the area was undergoing a vertical axis 30-40°
223 clockwise rotation (Fig.5C). This rotation agrees with the Bartonian-Priabonian clockwise rotation of
224 15-50° around a vertical-axis identified from paleomagnetism (Pueyo et al., 2002). The field study also
225 revealed bed-perpendicular joints oriented N160°E and N-S trending normal faults related to local outer-
226 arc extension during folding (Fig.5C). The fracturing history ends with the formation of N-S trending
227 reverse faults and transpressional reactivation of earlier ENE trending joints reflecting LSFT under an
228 E-W compression resulting from the local rotation of the regional NE-SW compression (Beaudoin et
229 al., 2015), followed by post-folding E-W trending reverse faults that formed under the same late N-S
230 compression than the Guarga thrust (Fig.5C).

231 U-Pb dating of calcite cements reveals that the veins related to NE-SW directed LPS formed as
232 early as ~61 ± 3 Ma ago, while late oblique-slip reverse faults (LSFT) and post-folding E-W reverse
233 faults were dated 19 ± 5 Ma and 18-14 ± 3 Ma, respectively (Hoareau et al., 2021). LPS, folding and
234 LSFT therefore lasted ~19 My (61-42 Ma), ~7 My (42-35 Ma) and ~17 My (35-18 Ma), respectively
235 (Fig.5D).

236

237 *3.3 Sheep Mountain Anticline (Rocky Mountains)*

238 The Sheep Mountain anticline is a thrust-related, basement-cored NW-SE striking fold that
239 developed in the Bighorn basin (Figs. 6A and B) during the late Cretaceous-Paleogene Laramide

contraction. Three main joint/vein sets were recognized (Fig. 6C, Bellahsen et al., 2006; Amrouch et al., 2010; Barbier et al., 2012). Set I consists of bed-perpendicular, WNW-ESE oriented veins associated with tectonic stylolites with ~WNW-ESE horizontal peaks (after unfolding) (Amrouch et al., 2010a, 2011). This set formed prior to folding under an horizontal σ1 trending WNW-ESE likely transmitted from the distant thin-skinned Sevier orogen at the time the Bighorn basin was still part of the Sevier undeformed foreland. Set II comprises vertical, bed-perpendicular joints/veins striking NE-SW, i.e., perpendicular to the fold axis. These veins are associated with tectonic stylolites with horizontal peaks oriented NE-SW and witness a NE-SW directed LPS (Varga, 1993; Amrouch et al., 2010a; Weil and Yonkee, 2012). The joints/veins of set III are bed-perpendicular and abut or cut across the veins of the former sets. They strike NW-SE parallel to the fold axis and their distribution mainly at the hinge zone of the fold support that they developed during outer-arc extension at the hinge of the growing anticline (Fig.6C). Widespread reverse and strike-slip faults also formed during LPS and LSFT, while bedding-parallel slip surfaces developed during fold growth (Amrouch et al., 2010a).

Veins from sets I, II and III were dated by means of U-Pb (Beaudoin et al., 2018). Set I veins yielded ages between 81 and 72 Ma, supporting their pre-Laramide formation. The Laramide LPS-related veins were dated 72–50 Ma. The age of set III veins constrains the timing of folding in the absence of preserved growth strata to 50–35 Ma (Beaudoin et al., 2018). Laramide LPS and fold growth therefore lasted ~20-25 My and ~15 My, respectively (Fig. 6D). The duration of the LSFT is poorly constrained, being bracketed between 35 Ma and the onset of the Basin and Range extension and Yellowstone hot-spot activity at ~17 Ma (Camp et al., 2015, Fig. 6D).

4. Discussion and conclusion

Absolute dating of mesostructures definitely confirms the sequence of deformation usually deduced from orientation data and relative chronology with respect to bedding attitude, and which includes LPS, fold growth (e.g., strata tilting) and LSFT (Fig.1). This sequence is valid for the four folds studied, despite San Vicino, Cingoli and Pico del Aguila anticlines developed above a decollement in a fold-and-thrust belt while Sheep Mountain anticline formed as a basement-cored forced fold above a basement thrust. The overall consistency between ages of growth strata when preserved, time constraints

derived from our multi-proxy analysis coupling isotopic geochemistry of cements and stylolite paleopiezometry, and U-Pb ages on early-, syn- and late-folding mesostructures demonstrates the reliability of our approach. Minor age overlaps are observed only when the duration of each deformation stage was shorter than age uncertainties, i.e. in the case of recent and rapid deformation (San Vicino and Cingoli, Fig.3F). Note that age overlaps could also relate with the fact that LPS and fold growth may overlap in some cases, as documented in the Sibillini thrust anticline, i.e. the southern continuation of the San Vicino anticline (Tavani et al., 2012).

Whatever the case, fold growth for the four folds lasted between 1.5 Ma and 15 Ma, in accordance with previous estimates of fold growth duration elsewhere using either syntectonic sedimentation (Holl and Anastasio, 1993; Anastasio et al., 2018) or mechanical modeling (Yamato et al., 2011). Moreover, our study quantifies for the first time the duration of the contraction before and after fold growth, and unexpectedly reveals that LPS and LSFT, albeit associated with lower amounts of shortening but potentially to substantial - if not most of - small-scale rock damage, may have lasted much longer than fold growth itself. Such trend can be key for the understanding of the history of foreland basins, including strata mechanical evolution and past fluid flow dynamics (Roure et al., 2005; Beaudoin et al., 2014).

Dating precisely the onset of LPS, whatever the technique used (U-Pb geochronology or absolute thermometry of calcite cements of mesostructures) is difficult as the entire range of vein ages may not be captured with certainty due to limited sampling. However, the onset of LPS can also be further constrained either by the sedimentary record of the foreland flexure preceding contraction (San Vicino) or by the estimate of the time at which vertical compaction-related pressure solution along bedding-parallel stylolites halted in the rocks in response to the switch of $\sigma 1$ axis from vertical to horizontal (Cingoli). The end of LSFT is also difficult to constrain precisely, but an upper bound is given by the change from fold-related shortening to a new regional state of stress. The latter is illustrated by the onset of post-orogenic extension in eastern UMAR (Fig.3), by the late Pyrenean compression in the Pico del Aguila area (Fig. 5) and by the Basin and Range extension in the Laramide province (Fig.6).

The four examples of folds also show that the overall duration of the folding event is variable (Fig.7). Fold growth lasted longer in the case of forced folding above a high angle basement thrust (Sheep Mountain) compared to fault-bend folding (San Vicino and Cingoli) along a flat-ramp decollement and detachment folding (Pico del Aguila) above a weak detachment layer in the cover (Fig. 5). The rapid fold growth and the relatively short LSFT in San Vicino and Cingoli are in line with the high rates of contraction and migration of deformation in the Apennines (Calamita et al., 1994, Fig .7). In contrast, LSFT appears longer when folding is anchored to a high angle basement thrust or when the fold is located at the front of the orogenic wedge, i.e., when the later propagation of deformation is limited or slow, or when it occurs in a complex sequence (Pico del Aguila and Sheep Mountain, Fig.7). The duration of LPS reflects to some degree the duration of the stress/strain accumulation in rocks required to generate folding, which can depend on the structural style (Beaudoin et al., 2020c). Our results support that a longer LPS (and a higher level of differential stress as well) is required to cause the inversion of a high angle basement normal fault and related forced folding of the undetached sedimentary cover (Sheep Mountain) than to initiate folding of the cover above a weak decollement (Pico del Aguila, Cingoli and San Vicino, Fig. 7). The longer LPS at Pico del Aguila compared to San Vicino and Cingoli (Fig.7) likely reflects the longer accumulation of displacement required to initiate folding oblique to the regional compression rather than perpendicular to it. It is worth to note that at first glance the fracture pattern (eg, Tavani et al., 2015) remains basically similar whatever the overall duration of the folding event and related deformation stages.

In summary, beyond regional implications, this study demonstrates that pre-, syn- and post-tilting mesostructures that formed under the same contraction than folding can be successfully dated. Our results bring for the first time absolute time constraints on the age and duration on the entire folding event for several upper crustal folds formed in different contractional settings. In particular, we not only better constrain the age and duration of fold growth, but also the onset and duration of the layer-parallel shortening stage that predates folding, and the duration and end of the late stage fold tightening. Because the duration of each of the deformation stages is found to depend on structural style and regional sequence of deformation, our results emphasize the need to more carefully consider the entire folding

event for a better appraisal of folding processes and stress/strain evolution in orogenic forelands, and for a more accurate prediction of host rock damage in naturally fractured reservoirs in folded domains.

Acknowledgements

NB is funded through the ISITE program E2S, supported by ANR PIA and Region Nouvelle- Aquitaine. The authors would like to thank the two anonymous reviewers for their constructive comments, as well as Fabrizio Storti, Catherine Mottram and Stephen Marshak for their comments on an earlier version of the manuscript.

Figure captions

Fig.1. Concept of folding event and associated mesostructures and growth strata.

Fig.2. Principle of dating of mesostructures related to the folding event. A. Photograph of a sedimentary stylolite cut by a vertical vein related to layer-parallel shortening (LPS). B. Principle of dating calcite veins using LA-ICP-MS, with laser ablation spots and final Tera-Wasserburg diagram. C. Principle of inversion of the roughness of sedimentary stylolites for stress. σ_v is the vertical stress, $\alpha = \frac{(1-2\nu)*(1+\nu)^2}{30\pi(1-\nu)^2}$, γ is the solid-fluid interfacial energy, ν is the Poisson ratio, E is the Young modulus, ρ is the dry density, g is the gravitational field acceleration and z is the depth. D. Principle of the combination of U-Pb dating and absolute $\Delta 47$ thermometry of calcite cements (here for LPS-related veins) with maximum depth of burial-related dissolution from sedimentary stylolites and burial-time evolution of strata to derive the timing of deformation stages during the folding event. Regional data are from Mazzoli et al., 2002 (flexure), Calamita et al. 1994 (folding and thrusting), Beaudoin et al., 2020b (LSFT).

Fig.3. San Vicino and Cingoli anticlines: A: location (AS: Adriatic Sea; TS: Tyrrhenian Sea). B: Cross section (after Mazzoli et al., 2002). C: Orientation of the main sets of mesostructures (relative chronology, 1 to 3), reported in current or unfolded attitude on a lower hemisphere Schmidt stereonet, and associated paleostress evolution. * denotes mesostructures dated using U-Pb. D: Burial model of

Cingoli constructed considering thickness from stratigraphic and well data corrected for chemical and physical compaction (modified from Labeur et al., 2021). The range of depths reconstructed from sedimentary stylolite roughness inversion (with uncertainty shaded in light grey) are reported for each formation as grey levels. The results of clumped isotope analysis (i.e., temperatures of precipitation of vein cements at thermal equilibrium with the host rock) are reported for LPS-related veins (blue) and syn-folding veins (red). The deduced timing of the deformation stages is reported. E: Age dating results for veins from San Vicino anticline: Tera-Wasserburg concordia plots for carbonate samples showing $^{238}U/^{206}Pb$ vs $^{207}Pb/^{206}Pb$ for veins of sets I (LPS-related) and III (LSFT-related)(n—no. of spots). MSWD—mean square of weighted deviates. F: Timing and duration of deformation stages. Color code for C and F: dark blue: flexure-related extension. blue: layer-parallel shortening (LPS); red: fold growth; green: late stage fold tightening (LSFT); yellow: post-folding extension.

Fig.4. 2D scans of veins dated by LA-ICP-MS U-Pb geochronology from San Vicino anticline, with location of the ablation spots and diagenetic state observed under cathodoluminescence microscopy. A: sample A16 (LPS-related vein). B: sample A19 (syn-folding vein). C: sample A20 (LSFT-related vein).

Fig.5. Pico del Aguila anticline: A: location (AB: Aquitaine Basin, JB: Jaca Basin, EB: Ebro Basin, PAZ: Pyrenean Axial Zone; P: Paleozoic; M: Mesozoic: C: Cenozoic). B: Cross sections (north after Poblet et al., 1997, south after Beaudoin et al., 2015). C: Orientation of the main sets of mesostructures (relative chronology, 1 to 5), reported in current or unfolded attitude on a lower hemisphere Schmidt stereonet (same key as Fig.3), and associated structural and paleostress evolution. Block diagrams modified after Beaudoin et al. (2015). * denotes mesostructures dated using U-Pb. D: Timing and duration of deformation stages. Color code for C and D : blue: layer-parallel shortening (LPS); red: fold growth; green: late stage fold tightening (LSFT); yellow: post-folding compression.

Fig.6. Sheep Mountain anticline: A: location (BHB: Bighorn Basin; WRB: Wind River Basin; PRB: Powder River Basin; GGB: Greater Green River Basin; DB: Denver Basin). B: Cross section (after Amrouch et al., 2010); C: Orientation of the main sets of veins (relative chronology, 1 to 3), shown on a field photograph and on a block-diagram of the final fold geometry, reported in unfolded attitude on a lower hemisphere Schmidt stereonet (same key as Fig.3), and associated structural and paleostress evolution. * denotes mesostructures dated using U-Pb. D: Timing and duration of the deformation stages. Color code for C and D: grey: pre-folding layer-parallel shortening kinematically unrelated to folding; blue: layer-parallel shortening (LPS); red: fold growth; green: late stage fold tightening (LSFT); yellow: post-folding extension.

Fig.7. Compared durations of the stages of the folding event, fold style (= final fold geometry) and sequence of regional deformation for the four studied folds (circled numbers 1 to 6 : order of structural development, i.e., sequence of folding/thrusting, with corresponding ages in Ma (between parentheses), red : from this study; black : from the literature (Beaudoin et al., 2018 for Wyoming, Jolivet et al. 2007 for the Pyrenees, Calamita et al., 1994 and Curzi et al., 2020 for the Apennines). Color code: blue: layer-parallel shortening (LPS); red: fold growth; green: late stage fold tightening (LSFT); yellow: post-folding extension/compression.

References

Ahmadhadi, F., Daniel, J.M., Azzizadeh, M., Lacombe, O.: Evidence for pre-folding vein development in the Oligo-Miocene Asmari Formation in the Central Zagros Fold Belt, Iran, Tectonics, 27, 2008.

Amrouch, K., Lacombe, O., Bellahsen, N., Daniel, J. M., Callot, J. P.: Stress and strain patterns, kinematics and deformation mechanisms in a basement-cored anticline: Sheep Mountain Anticline, Wyoming, Tectonics, 29(1), TC1005, 2010a.

Amrouch, K., Robion, P., Callot, J. P., Lacombe, O., Daniel, J. M., Bellahsen, N., Faure, J. L.: Constraints on deformation mechanisms during folding provided by rock physical properties: a case study at Sheep Mountain anticline (Wyoming, USA), Geophysical Journal International, 182(3), 1105-1123, 2010b.

Amrouch, K., Beaudoin, N., Lacombe, O., Bellahsen, N., Daniel, J.M.: Paleostress magnitudes in folded sedimentary rocks, Geophysical Research Letters, 38, L17301, 2011.

Anastasio, D., Kodama, K., Parés, J.: Episodic deformation rates recovered from growth strata, Pyrenees, Search and Discovery Article, 30553, 2018.

Aubourg, C., Smith, B., Eshraghi, A., Lacombe, O., Authemayou, C., Amrouch, K., Bellier O., Mouthereau, F.: New magnetic fabric data and their comparison with palaeostress markers in the Western Fars Arc (Zagros, Iran): tectonic implications, Geological Society London Special Publications, 330(1), 97-120, 2010.

Barbier, M., Leprêtre, R., Callot, J. P., Gasparrini, M., Daniel, J. M., Hamon, Y., Lacombe O., Floquet, M.: Impact of fracture stratigraphy on the paleo-hydrogeology of the Madison Limestone in two basement-involved folds in the Bighorn basin,(Wyoming, USA). Tectonophysics, 576, 116-132, 2012.

Barchi, M.: The Neogene–Quaternary evolution of the Northern Apennines: crustal structure, style of deformation and seismicity, Journal of Virtual Explorer, 36, 2010.

Barnes P.M.: Active folding of Pleistocene unconformities on the edge of the Australian-Pacific plate boundary zone, offshore North Canterburry, New Zealand, Tectonics, 15, 623-640, 1996.

Beaudoin, N., Leprêtre, R., Bellahsen, N., Lacombe, O., Amrouch, K., Callot, J.P., Emmanuel, L., Daniel, J.M.: Structural and microstructural evolution of the Rattlesnake Mountain Anticline (Wyoming, USA): New insights into the Sevier and Laramide orogenic stress build-up in the Bighorn Basin, Tectonophysics, 576-577, 20–45, 2012.

Beaudoin, N., Koehn, D., Lacombe, O., Lecouty, A., Billi, A., Aharonov, E., Parlangeau, C.: Fingerprinting stress: Stylolite and calcite twinning paleopiezometry revealing the complexity of progressive stress patterns during folding-The case of the Monte Nero anticline in the Apennines, Italy, Tectonics, 35, 1687-1712, 2016.

Beaudoin, N., Lacombe, O., Roberts, N. M. W., Koehn, D.: U-Pb dating of calcite veins reveals complex stress evolution and thrust sequence in the Bighorn Basin, Wyoming, USA, Geology, 46, 1015-1018, 2018.

Beaudoin, N., Huyghe, D., Bellahsen, N., Lacombe, O., Emmanuel, L., Mouthereau, F., Ouahnon, L.: Fluid systems and fracture development during syn-depositional fold growth: example from the Pico del Aguila Anticline, Sierras Exteriores, Southern Pyrenees, Spain, Journal of Structural Geology, 70, 23-38, 2015.

Beaudoin, N., Lacombe, O., David, M.E., Koehn, D.: Does stress transmission in forelands depend on structural style? Distinctive stress magnitudes during Sevier thin-skinned and Laramide thick-skinned layer-parallel shortening in the Bighorn Basin (USA) revealed by stylolite and calcite twinning paleopiezometry, Terra Nova, 32, 225-233, 2020c.

Beaudoin, N., Labeur, A., Lacombe, O., Koehn, D., Billi, A., Hoareau, G., Boyce, A., John, C.M., Marchegiano, M., Roberts, N.M., Millar, I.L., Claverie, F., Pecheyran, C., Callot, J.P.: Regional-scale paleofluid system across the Tuscan Nappe - Umbria Marche Apennine Ridge (northern Apennines) as revealed by mesostructural and isotopic analyses of stylolite-vein networks, Solid Earth, 11, 4, 1617-1641,2020b

Beaudoin, N., Bellahsen, N., Lacombe, O., Emmanuel, L., Pironon, J.: Crustal-scale fluid flow during the tectonic evolution of the Bighorn Basin (Wyoming, USA), Basin Research, 26(3), 403-435, 2014.

Beaudoin N. E., Lacombe, O., Koehn, D., David, M.E., Farrell, N., Healy, D.: Vertical stress history and paleoburial in foreland basins unravelled by stylolite roughness paleopiezometry: Insights from bedding-parallel stylolites in the Bighorn Basin,Wyoming, USA, Journal of Structural Geology. 136, 104061, 2020a.

Bellahsen, N., Fiore, P., Pollard, D.D.: The role of fractures in the structural interpretation of Sheep Mountain Anticline, Wyoming, Journal of Structural Geology, 28, 850-867, 2006.

Bertotti, G., de Graaf, S., Bisdom, K., Oskam, B., Vonhof, H.B., Bezerra, F.H.R., Reijmer, J.J.G., Cazarin, C.L.: Fracturing and fluid-flow during post-rift subsidence in carbonates of the Jandaíra Formation, Potiguar Basin, NE Brazil, Basin Research, 29, 836-853, 2017.

Bons, P.D., Elburg, M.A., Gomez-Rivas, E.: A review of the formation of tectonicveins and their microstructures, Journal of Structural Geology, 43, 33–62, 2012.

Branellec, M., Callot, J. P., Nivière, B., Ringenbach, J. C.: The fracture network, a proxy for mesoscale deformation: Constraints on layer parallel shortening history from the Malargüe fold and thrust belt, Argentina, Tectonics, 34(4), 623-647, 2015.

Butler, R.W.H., Lickorish, W.H.: Using high-resolution stratigraphy to date fold and thrust activity: examples from the Neogene of south-central Sicily, Journal of the Geological Society, 154, 633–643, 1997.
Calamita, F., Cello, G., Deiana, G., Paltrinieri, W.: Structural styles, chronology rates of deformation, and time-space relationships in the Umbria-Marche thrust system (central Apennines, Italy), Tectonics, 13, 873-881, 1994.
Callot, J.P., Robion, P., Sassi, W., Guiton, M.L.E., Kallel, N., Daniel, J.M., Mengus, J.M., Schmitz, J.: Magnetic characterisation of folded aeolian sandstones: interpretation of magnetic fabric in diamagnetic rocks, Tectonophysics, 495, 230-245, 2010.
Camp V.E., Pierce K.L., Morgan L.A. : Yellowstone plume trigger for Basin and Range extension, and coeval emplacement of the Nevada–Columbia Basin magmatic belt, Geosphere, 1, 2; 203–225, 2015.
Caricchi, C., Aldega, L., Corrado, S. Reconstruction of maximum burial along the Northern Apennines thrust wedge (Italy) by indicators of thermal exposure and modeling, Geological Society of America Bulletin, 127, 428–442, 2015.
Carrigan, J.H., Anastasio D.J., Kodama K.P., Parés J.M.: Fault-related fold kinematics recorded by terrestrial growth strata, Sant Llorenç de Morunys, Pyrenees Mountains, NE Spain, Journal of Structural Geology, 91, 161-176, 2016.
Curzi, M., Aldega, L., Bernasconi, S. M., Berra, F., Billi, A., Boschi, C., Franchini S., Van der Lelij R, Viola G., Carminati, E.: Architecture and evolution of an extensionally-inverted thrust (Mt. Tancia Thrust, Central Apennines): Geological, structural, geochemical, and K–Ar geochronological constraints, Journal of Structural Geology, 136, 104059, 2020.
Craddock, J. P., Jackson, M., van der Pluijm, B. A., Versical, R. T.: Regional shortening fabrics in eastern North America: Far-field stress transmission from the Appalachian-Ouachita Orogenic Belt, Tectonics, 12(1), 257-264, 1993.
Cruset, D., Vergés, J., Albert, R., Gerdes, A., Benedicto, A., Cantarero, I., & Travé, A.: Quantifying deformation processes in the SE Pyrenees using U–Pb dating of fracture-filling calcites, Journal of the Geological Society, 177(6), 1186-1196, 2020.
Cruset, D., Vergés, J., Rodrigues, N., Belenguer, J., Pascual-Cebrian, E., Almar, Y., Perez-Caceres I., Macchiavelli C., Trave A., Beranoaguirre A., Albert R., Gerdes A., Messager, G.: U–Pb dating of carbonate veins constraining timing of beef growth and oil generation within Vaca Muerta Formation and compression history in the Neuquén Basin along the Andean fold and thrust belt, Marine and Petroleum Geology, 132, 105204, 2021.
Ebner, M., Koehn, D., Toussaint, R., Renard, F., Schmittbuhl, J.: Stress sensitivity of stylolite morphology, Earth and Planetary Science Letters, 277, 394-398, 2009.
Evans, M. A., Fischer, M. P.: On the distribution of fluids in folds: A review of controlling factors and processes, Journal of Structural Geology, 44, 2-24, 2012.
Grobe, A., von Hagke, C., Littke, R., Dunkl, I., Wübbeler F., Muchez P., Urai JL: Tectono-thermal evolution of Oman's Mesozoic passive continental margin under the obducting Semail Ophiolite: a case study of Jebel Akhdar, Oman, Solid Earth 10 (1), 149-175, 2019.
Guiton M.L., Sassi W., Leroy Y.,Gauthier B.D.: Mechanical constraints on the chronology of fracture activation in folded Devonian sandstones of the western Moroccal Anti-Atlas, Journal of Structural Geology, 25, 1317-1330, 2003.
Hansman, R.J., Albert, R., Gerdes, A., Ring, U.: Absolute ages of multiple generations of brittle structures by U-Pb dating of calcite, Geology, 46, 207-210, 2018.
Hnat, J. S., van der Pluijm, B. A.: Foreland signature of indenter tectonics: Insights from calcite twinning analysis in the Tennessee salient of the Southern Appalachians, USA, Lithosphere, 3(5), 317-327, 2011.
Hoareau, G., Crognier, N., Lacroix, B., Aubourg, C., Roberts, N.W., Niemi, N., Branellec, M., Beaudoin, N.E., Suárez Ruiz, I. : Combination of Δ47 and U-Pb dating in tectonic calcite veins unravel the last

pulses related to the Pyrenean Shortening (Spain), Earth and Planetary Science Letters, 553, 116636, 2021.
Hogan, P.J., Burbank, D.W.: Evolution of the Jaca piggyback basin and emergence of the external Sierras, southern Pyrenees. In: Friend, P.F., Dabrio, C.J. (Eds.), Tertiary Basins of Spain. Cambridge Univ. Press, 153-160, 1996.
Holl, J. E., Anastasio, D. J.: Paleomagnetically derived folding rates, southern Pyrenees, Spain, Geology, 21, 271-274, 1993.
Jolivet, M., Labaume, P., Monie, P., Brunel, M., Arnaud, N., Campani, M.: Thermochronology constraints for the propagation sequence of the south Pyrenean basement thrust system (France-Spain), Tectonics 26, TC5007, 2007.
Labeur, A., Beaudoin, N.E., Lacombe, O., Emmanuel, L., Petracchini, L., Daëron, M., Klimowicz, S., Callot, J.-P.: Burial-deformation history of folded rocks unraveled by fracture analysis, stylolite paleopiezometry and vein cement geochemistry: A case ctudy in the Cingoli Anticline (Umbria-Marche, Northern Apennines), Geosciences, 11, 135, 2021.
Lacombe, O., Bellahsen, N., Mouthereau, F.: Fracture patterns in the Zagros Simply Folded Belt (Fars, Iran): constraints on early collisional tectonic history and role of basement faults, Geological Magazine, 148(5-6), 940-963, 2011.
Lacombe, O., Amrouch, K., Mouthereau, F., Dissez, L.: Calcite twinning constraints on late Neogene stress patterns and deformation mechanisms in the active Zagros collision belt, Geology, 35, 263–266, 2007.
Lacombe, O., Malandain, J., Vilasi, N., Amrouch, K., Roure, F.: From paleostresses to paleoburial in fold–thrust belts: preliminary results from calcite twin analysis in the Outer Albanides, Tectonophysics 475, 128–141, 2009.
Lacombe, O.: Calcite twins, a tool for tectonic studies in thrust belts and stable orogenic forelands, Oil & Gas Science and Technology–Revue d'IFP Energies nouvelles, 65(6), 809-838, 2010.
Lacombe O., Tavani S., Soto R.: Into the deformation history of folded rocks, Special Issue, Tectonophysics, 576–577, 1-3, 2012.
Masaferro, J. L., Bulnes, M., Poblet, J., Eberli, G. P.: Episodic folding inferred from syntectonic carbonate sedimentation: the Santaren anticline, Bahamas foreland, Sedimentary Geology, 146, 11-24, 2002.
Mazzoli, S., Deiana, G., Galdenzi, S., Cello, G.: Miocene fault-controlled sedimentation and thrust propagation in the previously faulted external zones of the Umbria-Marche Apennines, Italy, EGU Stephan Mueller Special Publication Series, 1, 195-209, 2002.
Mottram, C. M., Parrish, R. R., Regis, D., Warren, C. J., Argles, T. W., Harris, N. B., Roberts, N. M.: Using U-Th-Pb petrochronology to determine rates of ductile thrusting: Time windows into the Main Central Thrust, Sikkim Himalaya, Tectonics, 34(7), 1355-1374, 2015.
Mueller K . Suppe J.: Growth of Wheeler Ridge anticline, California: geomorphic evidence for fault-bend folding behavior during earthquakes, Journal of structural geology, 19, 383-396, 1997.
Nuriel P., Weinberger R., Kylander-Clark A.R.C., Hacker B.R., Craddock J.P.: The onset of the Dead Sea transform based on calcite age-strain analyses, Geology 45 (7), 587-590, 2017.
Poblet, J., McClay, K., Storti, F., Munoz, J.A.: Geometry of syntectonic sediments associated with single-layer detachment folds, Journal of Structural Geology, 19, 369-381, 1997.
Poblet, J., Hardy, S.: Reverse modelling of detachment folds; application to the Pico del Aguila anticline in the south-central Pyrenees (Spain), Journal of Structural Geology 17, 1707-1724, 1995.
Pueyo, E.L., Millan, H., Pocoví, A.: Rotation velocity of a thrust: a paleomagnetic study in the External Sierras (Southern Pyrenees), Sedimentary Geology, 146, 191-208, 2002.
Riba, O.: Syntectonic unconformities of the Alto Cardener, Spanish Pyrenees: A genetic interpretation, Sedimentary Geology, 15, 213–233, 1976.
Roberts, N. M., Walker, R. J.: U-Pb geochronology of calcite-mineralized faults: Absolute timing of rift-related fault events on the northeast Atlantic margin, Geology, 44, 531-534, 2016.

Roberts, N. M. W., Drost, K., Horstwood, M. S. A., Condon, D. J., Chew, D., Drake, H., Milodowski, A. E., McLean, N. M., Smye, A. J., Walker, R. J., Haslam, R., Hodson, K., Imber, J., Beaudoin, N., Lee, J. K.: Laser ablation inductively coupled plasma mass spectrometry (LA-ICP-MS) U–Pb carbonate geochronology: strategies, progress, and limitations, Geochronology, 2, 33-61, 2020.

Roberts, N. M., Žák, J., Vacek, F., Sláma, J.: No more blind dates with calcite: Fluid-flow vs. fault-slip along the Očkov thrust, Prague Basin, Geoscience Frontiers, 12(4), 101143, 2021.

Rocher, M., Lacombe, O., Angelier, J., Chen H.W.: Mechanical twin sets in calcite as markers of recent collisional events in a fold-and-thrust belt: evidence from the reefal limestones of southwestern Taiwan, Tectonics 15, 984–996, 1996.

Rocher, M., Lacombe, O., Angelier, J., Deffontaines, B., Verdier, F.: Cenozoic folding and faulting in the south Aquitaine Basin (France): insights from combined structural and paleostress analyses, Journal of Structural Geology, 22, 627–645, 2000.

Rolland, A., Toussaint, R., Baud, P., Schmittbuhl, J., Conil, N., Koehn, D., Renard, F., Gratier, J.-P.: Modeling the growth of stylolites in sedimentary rocks, Journal of Geophysical Research: Solid Earth, 117, B06403, 2012.

Roure, F., Swennen, R., Schneider, F., Faure, J.L., Ferket, H., Guilhaumou, N., Osadetz, K., Robion, P., Vandeginste, V.: Incidence and Importance of Tectonics and Natural Fluid Migration on Reservoir Evolution in Foreland Fold-And-Thrust Belts, Oil & Gas Science and Technology, 60, 67–106, 2005.

Sassi, W., Guiton, M., Leroy, Y.M., Kallel, N., Callot, J.P., Daniel, J.M., Lerat, O., Faure, J.L.: Constraints on mechanical modelling of folding provided by matrix deformation and fracture network analysis: The case of Split Mountain (Utah, USA), Tectonophysics, 576-577, 197-215, 2012.

Schmittbuhl, J., Renard, F., Gratier, J. P., Toussaint, R.: Roughness of stylolites: implications of 3D high resolution topography measurements, Physical Review Letters, 93, 238501, 2004.

Schneider, S., Hammerschmidt, K., Rosenberg, C. L.: Dating the longevity of ductile shear zones: Insight from 40Ar/39Ar in situ analyses, Earth and Planetary Science Letters, 369, 43-58, 2013.

Shackleton, J. R., Cooke, M. L., Verges, J., Sima, T.: Temporal constraints on fracturing associated with fault-related folding at Sant Corneli anticline, Spanish Pyrenees, Journal of Structural Geology, 33(1), 5-19, 2011.

Storti, F., Poblet, J.: Growth stratal architectures associated to decollement folds and fault-propagation folds. Inferences on fold kinematics, Tectonophysics, 282(1-4), 353-373, 1997.

Suppe, J., Chou, G.T. and Hook, S.C.: Rates of folding and faulting determined from growth strata. In: McClay, K.R. (Ed.), Thrust Tectonics. Chapman & Hall, Suffolk, pp.105-121, 1992.

Tavani, S., Storti, F., Lacombe, O., Corradetti, A., Muñoz, J., Mazzoli, S.: A review of deformation pattern templates in foreland basin systems and fold-and-thrust belts: Implications for the state of stress in the frontal regions of thrust wedges, Earth-Science Reviews, 141, 82-104, 2015.

Tavani S., Storti F., Fernández O, Muñoz JA, Salvini F.: 3-D deformation pattern analysis and evolution of the Añisclo anticline, southern Pyrenees, Journal of Structural Geology, 28 (4), 695-712, 2006.

Tavani S., Storti F., Salvini F., Toscano C. : Stratigraphic versus structural control on the deformation pattern associated with the evolution of the Mt. Catria anticline, Italy, Journal of Structural Geology, 30 (5), 664-681, 2008.

Tavani S., Mencos J., Bausà J., Muñoz JA. : The fracture pattern of the Sant Corneli Bóixols oblique inversion anticline (Spanish Pyrenees), Journal of Structural Geology 33 (11), 1662-1680, 2011.

Tavani, S., Storti, F., Bausa, J., & Munoz, J. A.: Late thrusting extensional collapse at the mountain front of the northern Apennines (Italy), Tectonics, 31(4), 2012.

Toussaint, R., Aharonov, E., Koehn, D., Gratier, J. P., Ebner, M., Baud, P., Rolland, A., Renard, F.: Stylolites: A review, Journal of Structural Geology, 114, 163-195, 2018.

Varga, R.J.: Rocky Mountain foreland uplifts: products of a rotating stress field or strain partitioning? Geology, 21, 1115-1118, 1993.

Vermeesch, P.: Unifying the U–Pb and Th–Pb methods: joint isochron regression and common Pb correction, Geochronology, 2, 119-131, 2020.

Vidal-Royo, O., Koyi, H. A., & Muñoz, J.A.: Formation of orogen-perpendicular thrusts due to mechanical contrasts in the basal décollement in the Central External Sierras (Southern Pyrenees, Spain), Journal of Structural Geology, 31(5), 523-539, 2009.

Weil, A.B., Yonkee, W.A.: Layer-parallel shortening across the Sevier fold-thrust belt and Laramide foreland of Wyoming: spatial and temporal evolution of a complex geodynamic system, Earth and Planetary Science Letters, 357-358, 405-420, 2012.

Yamato, P., Kaus, B. J., Mouthereau, F., Castelltort, S.: Dynamic constraints on the crustal-scale rheology of the Zagros fold belt, Iran, Geology, 39, 815-818, 2011.

Wang Y., Zwingmann H., Zhou L., Lo C.-H.,Viola G., Hao J.: Direct dating of folding events by 40Ar/39Ar analysis of synkinematic muscovite from flexural-slip planes, Journal of Structural Geology, 83, 46-59, 2016.

Dataset availability: Data either are available as supplementary material or come from properly cited literature.

Author contribution: Conceptualization : O. Lacombe, N. Beaudoin; Data acquisition : all authors; Vizualization : O. Lacombe, N. Beaudoin, G. Hoareau, A. Labeur; Funding acquisition : N. Beaudoin; Writing – original draft preparation : O. Lacombe, N. Beaudoin; Writing – review and editing : O. Lacombe, N. Beaudoin, G. Hoareau, J.P. Callot

Competing interest: “The authors declare that they have no conflict of interest”

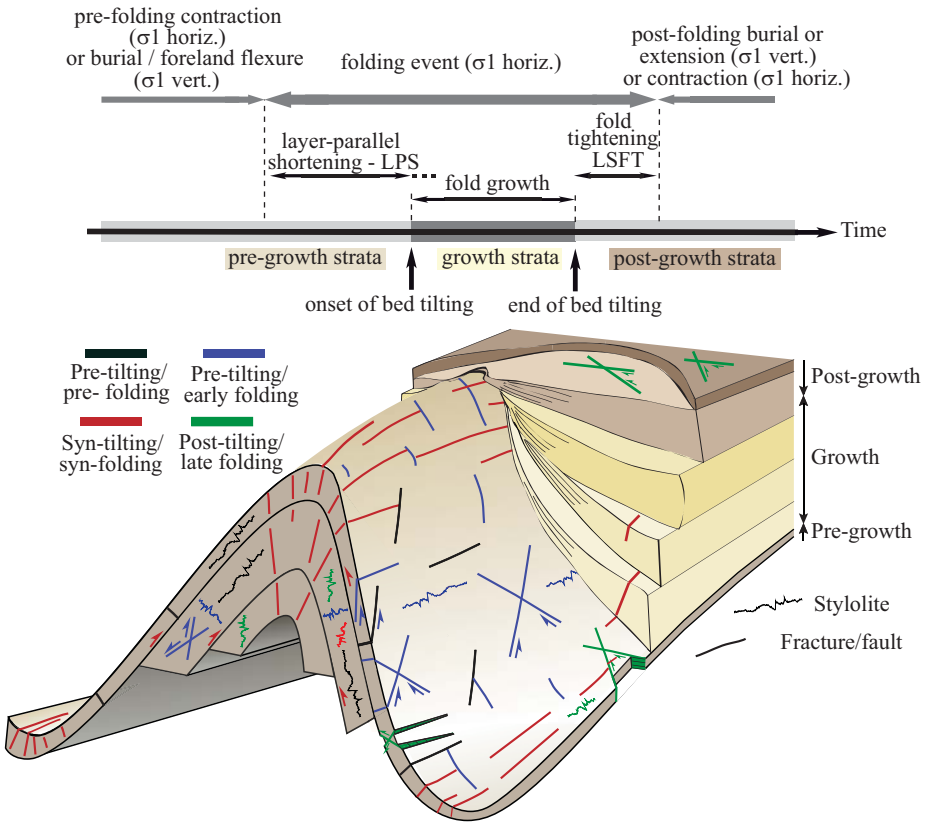

Fig.1. Concept of folding event and associated mesostructures and growth strata.

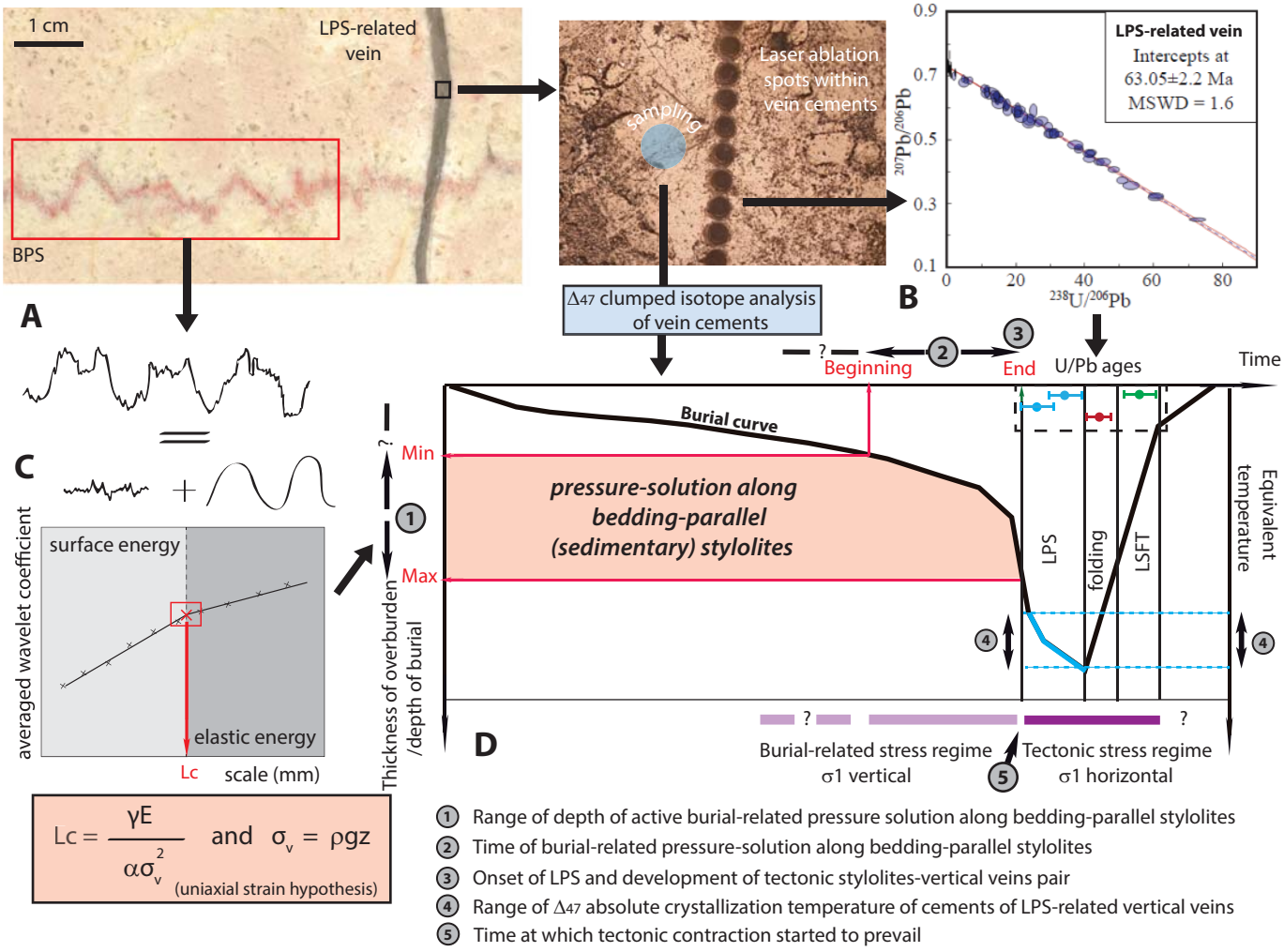

Fig.2. Principle of dating of mesostructures related to the folding event. A. Photograph of a sedimentary stylolite cut by a vertical vein related to layer-parallel shortening (LPS). B. Principle of dating calcite veins using LA-ICP-MS, with laser ablation spots and final Tera-Wasserburg diagram. C. Principle of inversion of the roughness of sedimentary stylolites for stress. σv is the vertical stress, $\alpha=((1-2\nu)*(1+\nu)^2)/(30\pi(1-\nu)^2)$, γ is the solid-fluid interfacial energy, ν is the Poisson ratio, E is the Young modulus, ρ is the dry density, g is the gravitational field acceleration and z is the depth. D. Principle of the combination of U-Pb dating and absolute Δ47 thermometry of calcite cements (here for LPS-related veins) with maximum depth of burial-related dissolution from sedimentary stylolites and burial-time evolution of strata to derive the timing of deformation stages during the folding event.

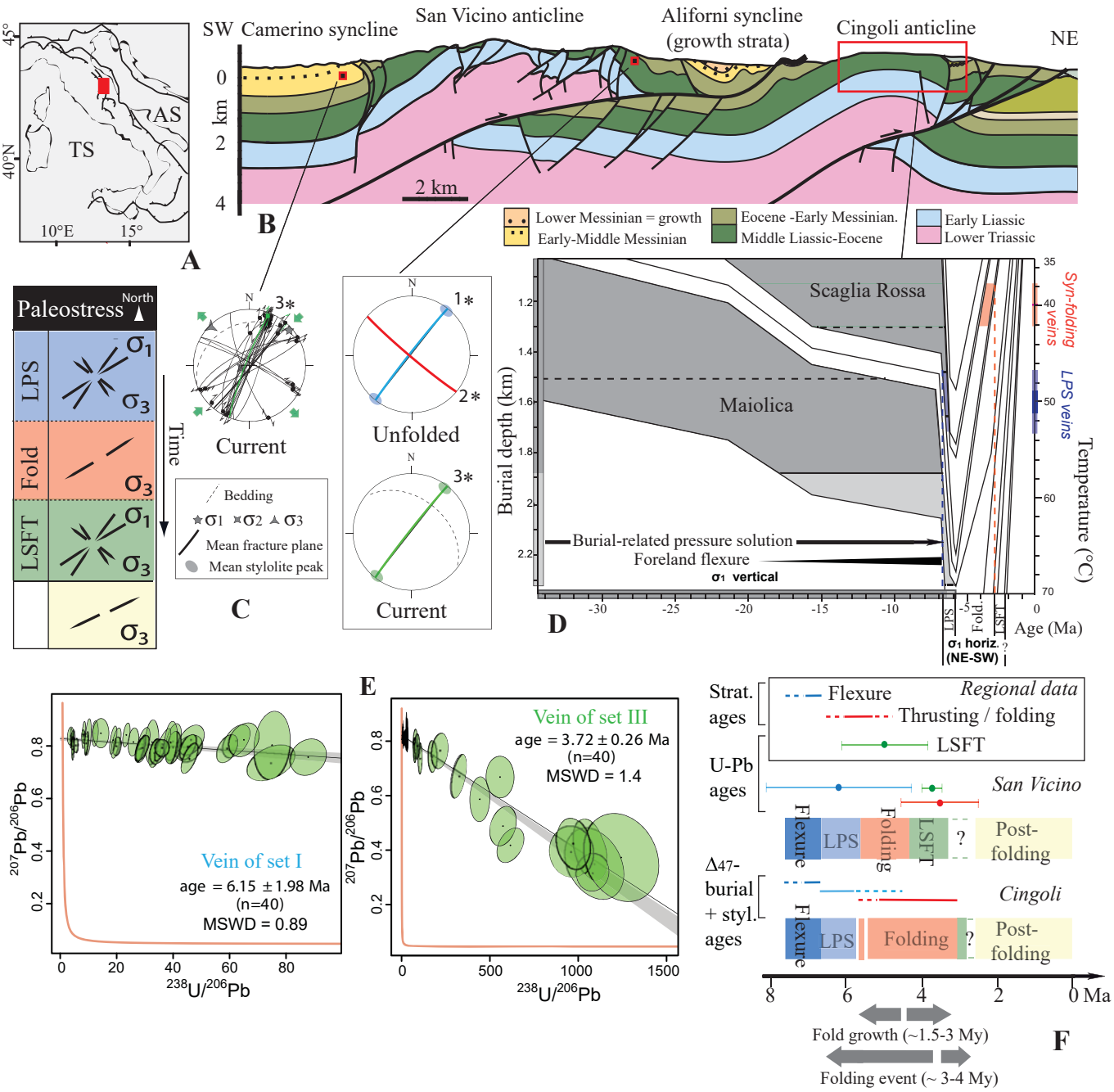

Fig.3. San Vicino and Cingoli anticlines: A: location (AS: Adriatic Sea; TS: Tyrrhenian Sea). B: Cross section (after Mazzoli et al., 2002). C: Orientation of the main sets of mesostructures (relative chronology, 1 to 3), reported in current or unfolded attitude on a lower hemisphere Schmidt stereonet, and associated paleostress evolution. * denotes mesostructures dated using U-Pb. D: Burial model of Cingoli constructed considering thickness from stratigraphic and well data corrected for chemical and physical compaction (modified from Labeur et al., 2021). The range of depths reconstructed from sedimentary stylolite roughness inversion (with uncertainty shaded in light grey) are reported for each formation as grey levels. The results of clumped isotope analysis (i.e., temperatures of precipitation of vein cements at thermal equilibrium with the host rock) are reported for LPS-related veins (blue) and syn-folding veins (red). The deduced timing of the deformation stages is reported. E: Age dating results for veins from San Vicino anticline: Tera-Wasserburg concordia plots for carbonate samples showing 238U/206Pb vs 207Pb/206Pb for veins of sets I (LPS-related) and III (LSFT-related) (n—no. of spots). MSWD—mean square of weighted deviates. F: Timing and duration of deformation stages. Regional data are from Mazzoli et al., 2002 (flexure), Calamita et al. 1994 (folding and thrusting), Beaudoin et al., 2020c (LSFT). Color code for C and F: dark blue: flexure-related extension. blue: layer-parallel shortening (LPS); red: fold growth; green: late stage fold tightening (LSFT); yellow: post-folding extension.

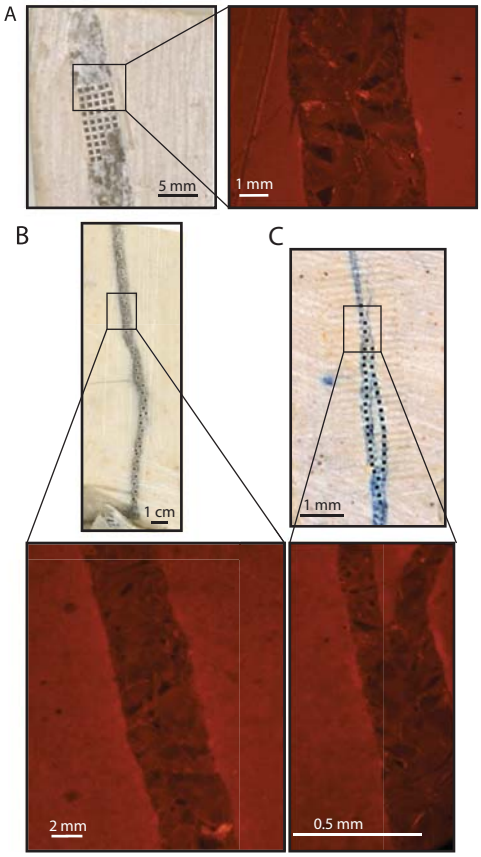

Fig.4. 2D scans of veins dated by LA-ICP-MS U-Pb geochronology from San Vicino anticline, with location of the ablation spots and diagenetic state observed under cathodoluminescence microscopy. A: sample A16 (LPS-related vein). B: sample A19 (syn-folding vein). C: sample A20 (LSFT-related vein).

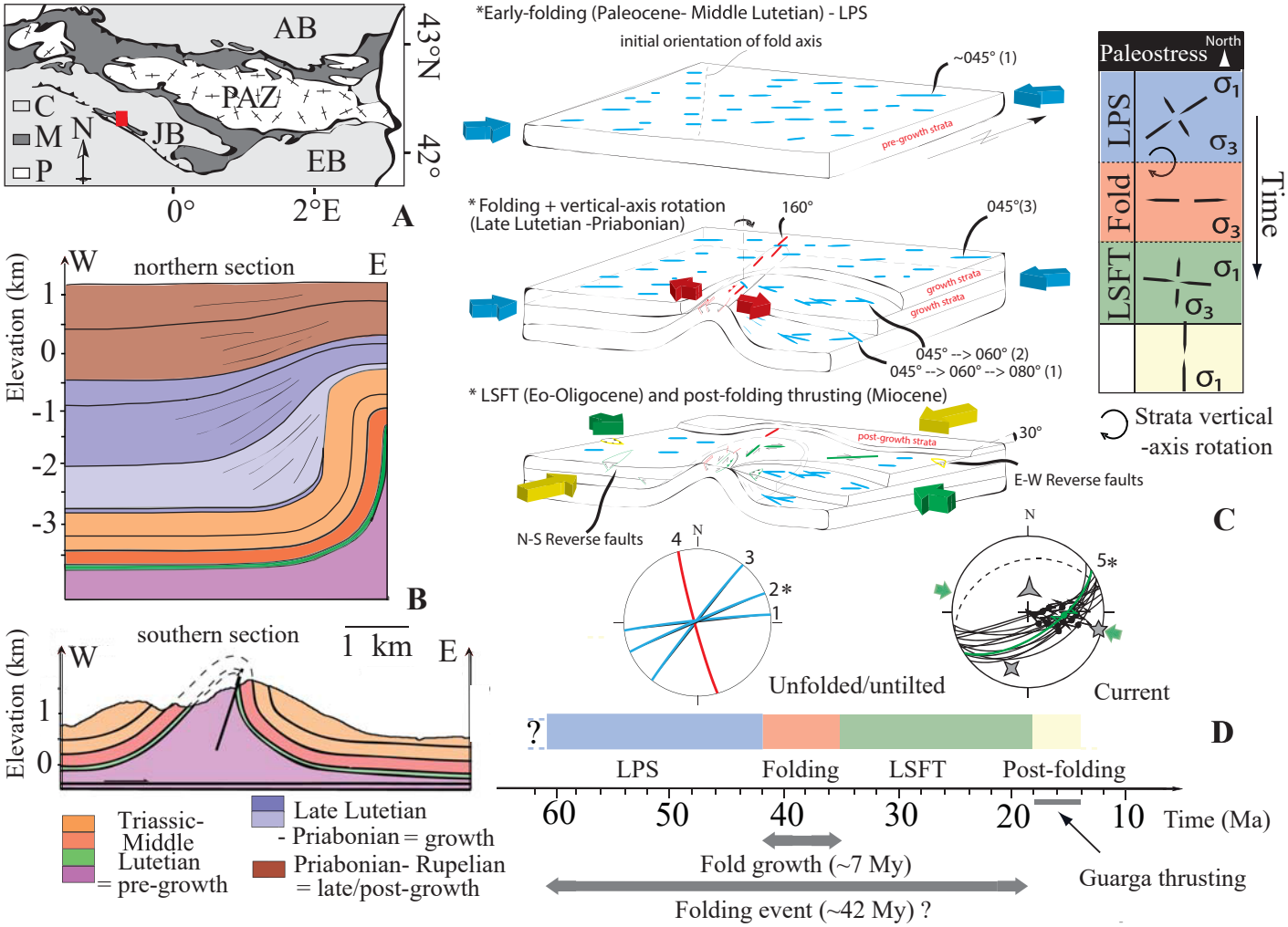

Fig.5. Pico del Aguila anticline: A: location (AB: Aquitaine Basin, JB: Jaca Basin, EB: Ebro Basin, PAZ: Pyrenean Axial Zone; P: Paleozoic; M: Mesozoic: C: Cenozoic). B: Cross sections (north after Poblet et al., 1997, south after Beaudoin et al., 2015). C: Orientation of the main sets of mesostructures (relative chronology, 1 to 5), reported in current or unfolded attitude on a lower hemisphere Schmidt stereonet (same key as Fig.3), and associated structural and paleostress evolution. Block diagrams modified after Beaudoin et al. (2015). * denotes mesostructures dated using U-Pb. D : Timing and duration of deformation stages. Color code for C and D : blue: layer-parallel shortening (LPS); red: fold growth; green: late stage fold tightening (LSFT); yellow: post-folding compression.

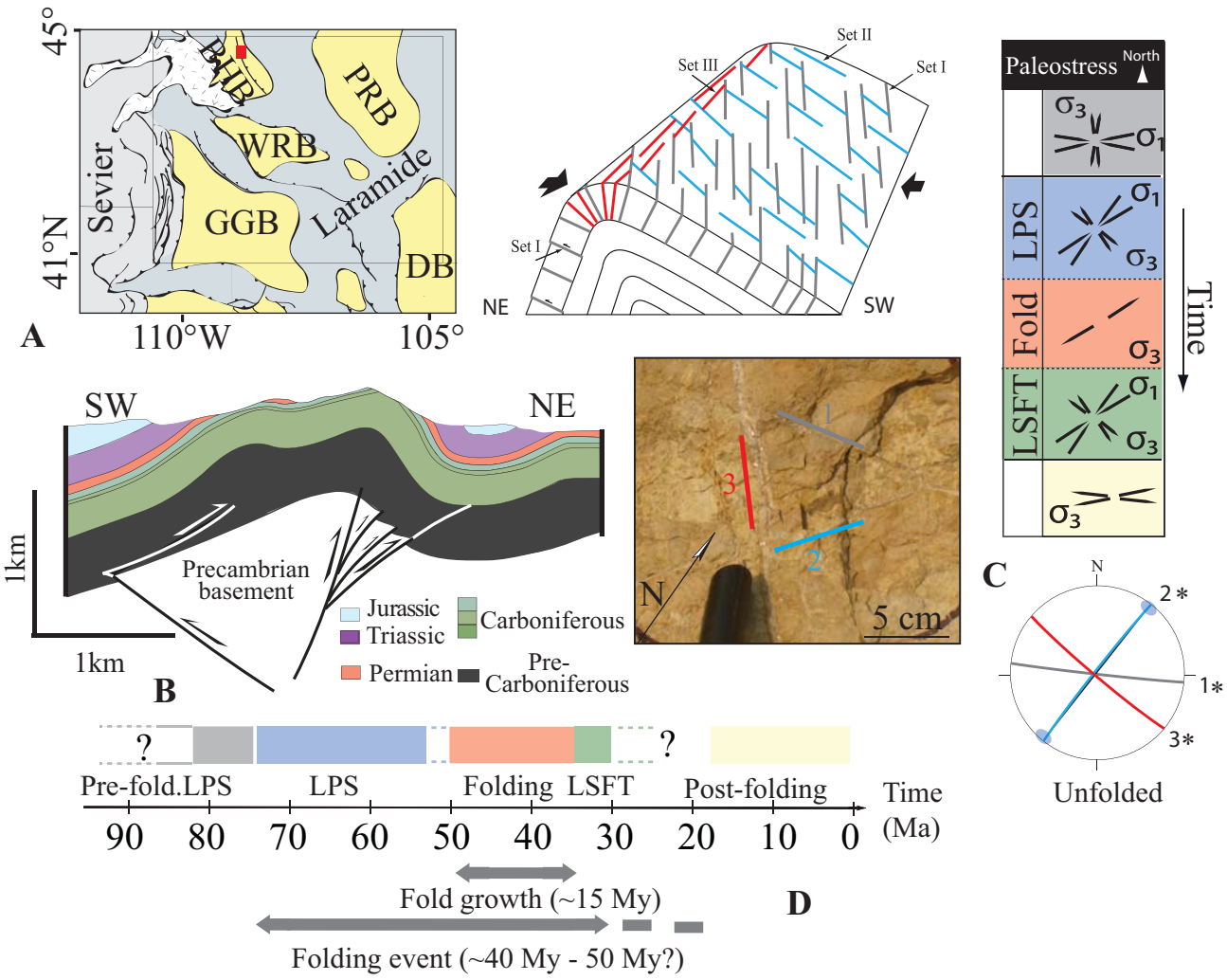

Fig.6. Sheep Mountain anticline: A: location (BHB: Bighorn Basin; WRB: Wind River Basin; PRB: Powder River Basin; GGB: Greater Green River Basin; DB: Denver Basin). B: Cross section (after Amrouch et al., 2010); C: Orientation of the main sets of veins (relative chronology, 1 to 3), shown on a field photograph and on a block-diagram of the final fold geometry, reported in unfolded attitude on a lower hemisphere Schmidt stereonet (same key as Fig.3), and associated structural and paleostress evolution. * denotes mesostructures dated using U-Pb. D: Timing and duration of the deformation stages. Color code for C and D : grey: pre-folding layer-parallel shortening kinematically unrelated to folding; blue: layer-parallel shortening (LPS); red: fold growth; green: late stage fold tightening (LSFT); yellow: post-folding extension.

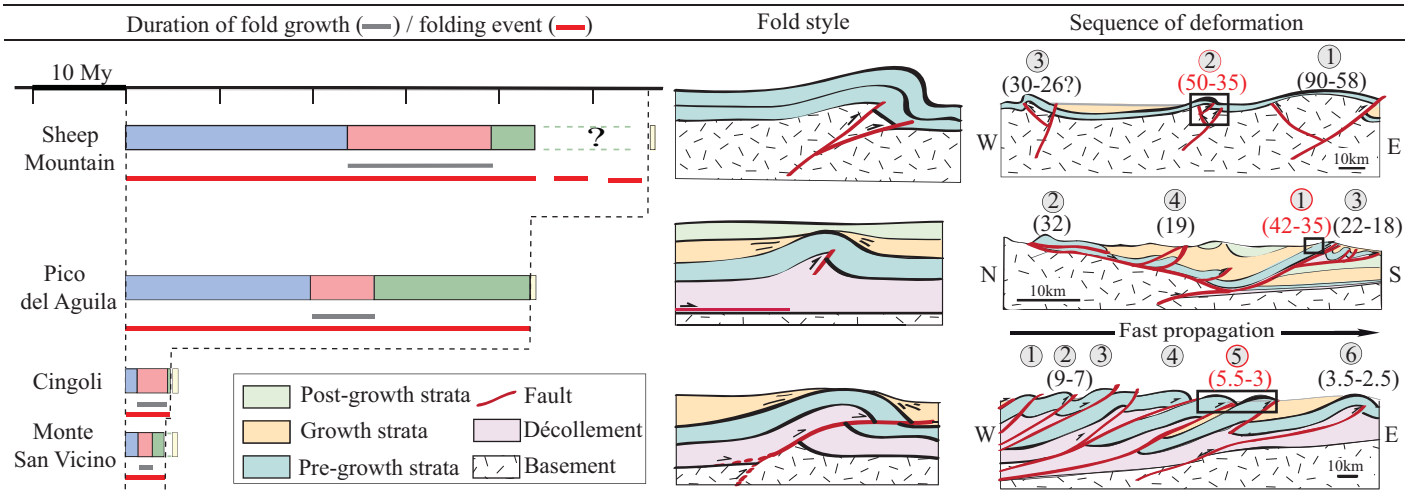

Fig.7. Compared durations of the stages of the folding event, fold style (= final fold geometry) and sequence of regional deformation for the four studied folds (circled numbers 1 to 6 : order of structural development, i.e., sequence of folding/thrusting, with corresponding ages in Ma (between parentheses), red : from this study; black : from the literature (Beaudoin et al., 2018 for Wyoming, Jolivet et al. 2007 for the Pyrenees, Calamita et al., 1994 and Curzi et al., 2020 for the Apennines). Color code: blue: layer-parallel shortening (LPS); red: fold growth; green: late stage fold tightening (LSFT); yellow: post-folding extension/compression.